Electronic Journal of Structural Engineering

Original Article

Cite this: DOI:10.56748/ejse.26990

Received Date: 28 March 2026
Accepted Date: 26 July 2026

1443-9255
https://ejsei.com/ejse

Improving Composite Action in Circular CFST Columns Using Internal Spiral Plates

Sandeep T N [a*], **Job Thomas** [a]

[a] School of Engineering, Cochin University of Science and Technology, Kerala, India
* Corresponding author: sandeeptncivil@gmail.com

Abstract

Numerous confinement techniques have been proposed to enhance the strength and ductility of circular concrete-filled steel tube (CFST) columns. This study introduces an innovative confinement method for short circular CFST columns incorporating internal spiral plate stiffeners. The rectangular spiral plates are attached to the inner surface of the steel tube such that their flat faces remain in direct contact with the tube wall. This configuration minimizes obstruction to concrete flow and ensures proper compaction without void formation during casting. The spiral plates were connected to the steel tube using intermittent external fillet welding and tested under axial compression to evaluate their influence on load-carrying capacity and deformation behavior. A detailed finite element (FE) model was developed to complement the experimental program and to investigate the effects of key parameters, including spiral pitch, plate width, and weld spacing, on axial performance. The results demonstrate that incorporating spiral plate stiffeners increases the ultimate strength by an average of 16% compared to conventional CFST columns. Strength enhancement ranged from 5% to 55% as the spiral pitch decreased from 150 mm to 25 mm, while reducing weld spacing from 180° to 30° improved strength by 6–10%. A normalized spiral pitch (p/D) ≤ 0.5 provided effective confinement, resulting in stable post-peak behavior and mitigation of local buckling. Increasing the spiral plate width up to 40 mm enhanced axial strength by approximately 22%, highlighting its contribution to improved load resistance. Furthermore, the spiral plates were effectively delayed and uniformly distributed local bulging along the column height.

Keywords

Concrete-filled steel tube (CFST) column, Finite element analysis (FEA), Confined CFST column, Spiral plate stiffener

1. Introduction

Concrete-filled steel tube (CFST) columns have gained widespread acceptance in modern construction due to their superior structural efficiency and practical advantages. Extensive research has demonstrated that CFST columns exhibit significantly higher load-carrying capacity and ductility compared to conventional reinforced concrete or bare steel columns (Giakoumelis and Lam, 2004; Guptha et al., 2014, 2015; Hoang and Fehling, 2017; Hamed et al., 2021; Guptha et al, 2022; Lyu et al., 2024). The composite interaction between the steel tube and the concrete core enables effective confinement of the concrete and delay of local buckling of the steel tub. Several studies have examined the confinement mechanism in CFST columns. Dabaon et al. (2009), de Oliveira et al. (2010), Nematzadeh and Fazli (2020), Abbas and Ali (2021), and Hu et al. (2024) demonstrated that the steel tube provides lateral confinement to the concrete core, and that increasing the degree of confinement substantially enhances both strength and ductility. In addition to confinement, the bond interaction at the steel–concrete interface plays a critical role in composite action. Midhin et al. (2020) and Naghipour et al. (2022) reported that interfacial delamination may occur during the early stages of loading, which can adversely affect structural performance. To further enhance composite action, researchers have proposed various strengthening and confinement techniques. These include external rings, external spirals, tie bars, steel jackets, CFRP wrapping, and shear studs. Lai and Ho (2014, 2015) and Ho et al. (2016) demonstrated that external rings and spirals effectively restrain lateral expansion of the core concrete, thereby improving axial behavior. Tie bars were shown to enhance axial capacity (Lai and Ho, 2014; Alrebeh et al., 2023), while steel jackets provide an alternative to welding and offer efficient confinement (Lai and Ho, 2015). CFRP wrapping has also been widely investigated as an external confinement method, with significant improvements in strength and ductility reported by Hu et al. (2011), Prabhu and Sundarraja (2013), and Chen et al. (2023). Furthermore, Huang et al. (2002) and Arokiaprakash & Selvan (2022) demonstrated that shear studs considerably improve bond performance between the steel tube and concrete core. Internal stiffening techniques have also received considerable attention. Tao et al. (2007, 2009), Dabaon et al. (2009), Winti et al. (2026) and Zhu et al. (2026) investigated various forms of internal stiffeners to improve bond interaction and delay local buckling. Li et al. (2025) proposed semi-circle stiffened CFST columns, which exhibited enhanced confinement, strength, and ductility with delayed local buckling. Tao et al. (2005) proposed externally attached stiffener plates to enhance confinement, while Tao et al. (2008) introduced saw-shaped internal plate stiffeners that significantly improved post-buckling behavior. Petrus et al. (2010) further developed tab stiffeners, which enhanced mechanical interlocking between steel and concrete. A hybrid approach combining external rings with internal stiffeners was later proposed by Alrebeh and Ekmekyapar (2019a), demonstrating substantial improvement in axial load resistance.

Among recent developments, spiral confinement has emerged as an efficient technique for enhancing composite action (Lai and Ho, 2015; Lin and Zhou, 2023; Arokiaprakash and Senthil, 2023). Fig. 1(a) illustrates a typical external spiral confinement arrangement. Although effective, external spirals may raise aesthetic concerns in architectural applications. To overcome this limitation, Alrebeh and Ekmekyapar (2019b) introduced an internal spiral confinement system in which circular rods are installed as internal spirals within the steel tube, as shown in Fig. 1(b).

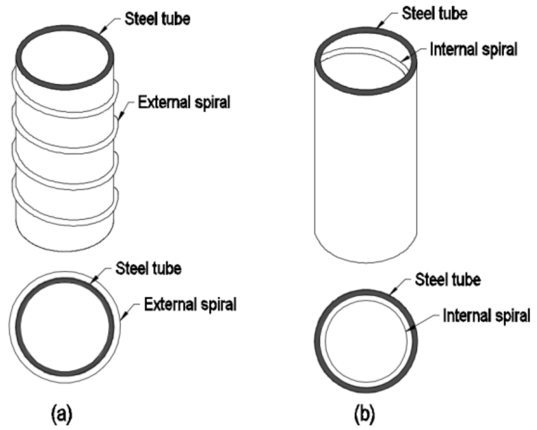

Fig. 1 (a) External spiral confined CFST column, (b) Internal spiral confined CFST column

Steel tubes in CFST columns may undergo outward local buckling under high axial compressive loads, which can lead to premature deterioration of structural capacity. Alrebeh and Ekmekyapar (2019b) and Tao et al. (2016) emphasized that the bond interaction between the steel tube and the concrete core plays a crucial role in governing the overall behavior of CFST columns. Loss of bond results in interfacial separation, forming a gap between the steel tube and the concrete core, as illustrated in Fig. 2(a). Furthermore, concrete shrinkage during curing may further weaken the interface, reducing the effectiveness of composite action, as shown in Fig. 2(b). To address these challenges, internal plate connectors can be welded to the inner surface of the steel tube. These plates function as mechanical interlocking elements, improving load transfer and enhancing bond strength between the steel tube and the concrete core. Consequently, the integrity of composite action is maintained, leading to improved axial load capacity, delayed local buckling, and enhanced overall structural performance of the column.

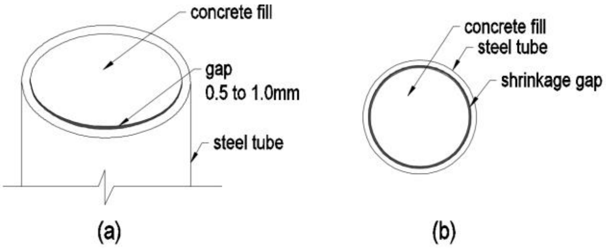

Fig. 2 (a) Slippage between steel tube and core concrete due to loading, (b) Shrinkage gap between steel tube and concrete

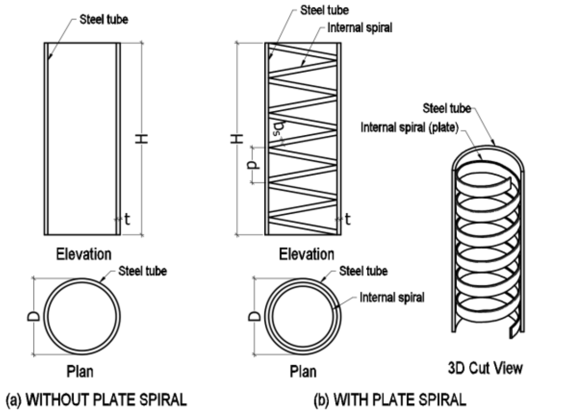

Fig. 3 Illustration of CFST column with and without internal plate spiral

To address the aforementioned challenges, namely, the need for an effective confinement mechanism and enhanced bonding between the steel tube and the concrete core, a novel confinement technique integrating both aspects is proposed in this study. The proposed system combines spiral confinement, recognized as one of the most efficient confinement methods, with internally welded stiffener plates to improve composite interaction. This research investigates the structural performance of short circular concrete-filled steel tube (CFST) columns incorporating internal spiral plate stiffeners. The spiral plate, having a rectangular cross-section, provides a larger contact surface with the core concrete compared to circular rod spirals, thereby enhancing both bond strength and confinement efficiency. Furthermore, the spiral plate is connected to the inner surface of the steel tube through intermittent external plug welding, following the recommendations of Thomas and Sandeep (2018, 2020). This welding configuration ensures reliable mechanical anchorage while maintaining fabrication simplicity. The intermittent weld arrangement enhances stress transfer between the steel tube and the confined concrete core, resulting in improved composite action. The geometric configuration of the CFST column strengthened with an internal spiral plate stiffener is illustrated in Fig. 3. To validate the proposed confinement technique, a combined experimental and numerical investigation was conducted. The experimental program provided direct insight into load–displacement behavior and confinement effectiveness under axial compression. Complementary finite element (FE) simulations enabled an extensive parametric study, examining the influence of spiral pitch, plate width, and weld spacing. The integration of experimental observations and numerical modeling ensured comprehensive validation of the proposed stiffening strategy.

2. Experimental Study

2.1 Specimen Preparation and Testing

A total of nine short circular concrete-filled steel tube (CFST) column specimens were fabricated and tested under axial compression. The steel tubes had an outer diameter of 113 mm and a uniform wall thickness of 2.0 mm. The specimens had a gross cross-sectional area of 10024 mm² and a slenderness ratio of 2.8. All tubes were fabricated from Fe 250 grade steel. Tensile coupon tests indicated a measured yield strength of 290 MPa and an ultimate tensile strength of 460 MPa. The concrete core was designed as M30 grade concrete, achieving a 28-day cube compressive strength of 36 MPa, determined using 150 mm standard cube specimens. The concrete mix incorporated 12 mm nominal maximum size coarse aggregates. A superplasticizer was added to ensure adequate workability and flowability during casting, particularly to facilitate proper filling around the internal spiral plates. Among the nine specimens, one served as the control specimen without internal stiffeners. The remaining specimens incorporated internal spiral plate stiffeners with different spiral pitch spacings of 25 mm, 50 mm, 75 mm, and 150 mm. Two plate cross-sectional sizes were used: 10 mm × 2 mm and 20 mm × 2 mm. The spiral plates were fabricated from steel with a yield strength of 260 MPa. The details of all specimens are summarized in Table 1. Specimens were designated using the notation CX–P, where C denotes a circular CFST column, X indicates the plate size (1 for 10 mm × 2 mm and 2 for 20 mm × 2 mm), and P represents the spiral pitch spacing in millimetres. For example, C1–25 represents a circular CFST column reinforced with 10 mm × 2 mm internal spiral plates at a pitch of 25 mm, whereas C–0 denotes the control specimen without spiral stiffeners. The steel tube dimensions were kept constants for all specimens, and only the spiral pitch and plate size were varied to evaluate their influence on confinement efficiency.

The spiral plates were bent into the required helical configuration using a mechanical bending machine to ensure dimensional accuracy and uniformity prior to installation. The plates were fixed to the inner surface of the steel tubes using intermittent plug welding through predrilled holes from the outer surface of the tube. A constant weld spacing of 90° along the tube circumference was maintained, resulting in four plug welds per spiral pitch. This welding configuration provided reliable mechanical anchorage between the stiffeners and the steel tube while maintaining fabrication practicality. The fabrication details of the test specimens are illustrated in Fig. 4. During casting, the steel tubes were positioned vertically and filled with fresh concrete in multiple layers. A needle vibrator was used to ensure proper compaction and eliminate entrapped air, thereby achieving a dense and homogeneous concrete core. Care was taken to maintain mix uniformity and prevent segregation of coarse aggregates. After casting, the specimens were covered with moist burlap and cured under controlled conditions for 28 days to ensure adequate hydration and strength development.

Table 1. Specimen Details and Properties

Sl No	Specimen ID	Stiffener Size, mm	Pitch, mm	Ultimate load, N_{exp}, kN	Strength ratio	Strain degradation rate x 10^{-6}
1	C-0	-	-	611	-	-4.0
2	C1-25	10×2	25	794	1.30	0.1
3	C1-50	10×2	50	721	1.18	-1.0
4	C1-75	10×2	75	666	1.09	-2.3
5	C1-150	10×2	150	623	1.02	-2.7
6	C2-25	20×2	25	948	1.55	0.8
7	C2-50	20×2	50	787	1.29	0.3
8	C2-75	20×2	75	692	1.13	-0.8
9	C2-150	20×2	150	640	1.05	-2.1

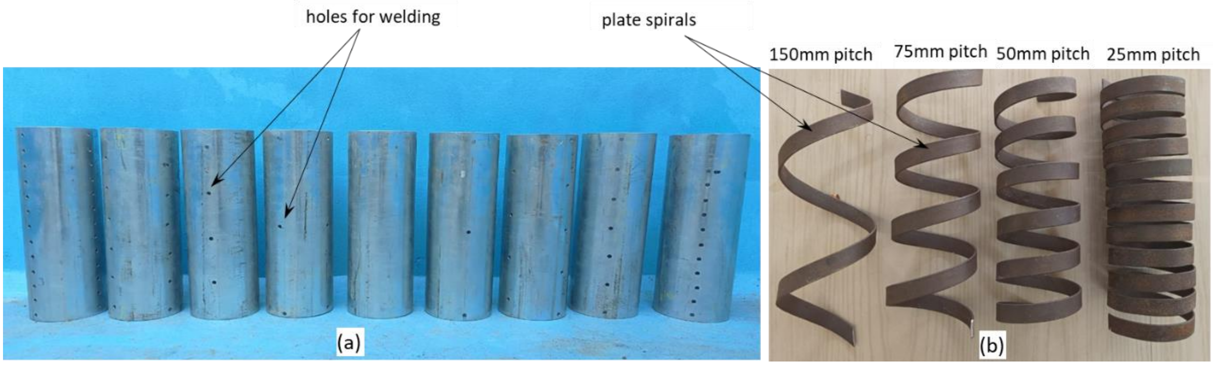

Fig. 4 Fabrication details of specimens (a) Steel tubes having weld holes (b) Plate spirals

All specimens were tested under axial compression using a Compression Testing Machine (CTM) with a maximum load capacity of 1000kN. A detailed instrumentation diagram illustrating the test setup is shown in Fig. 5. Each column was positioned vertically between the loading platens to simulate concentric axial loading conditions. To minimize seating irregularities and ensure uniform contact between the specimen ends and the machine platens, a small preliminary seating load was applied and subsequently released prior to the commencement of the actual test. This procedure ensured proper alignment and reduced the possibility of eccentric loading. The axial load was applied and increased monotonically until failure. Load and corresponding axial deformation were recorded continuously throughout the test. Axial shortening was measured using three dial gauges mounted symmetrically around the circumference of each specimen. Each dial gauge had the least count of 0.01 mm, ensuring accurate measurement of axial deformation. The use of three gauges allowed for verification of uniform deformation and helped detect any unintended eccentricity or localized deformation during loading.

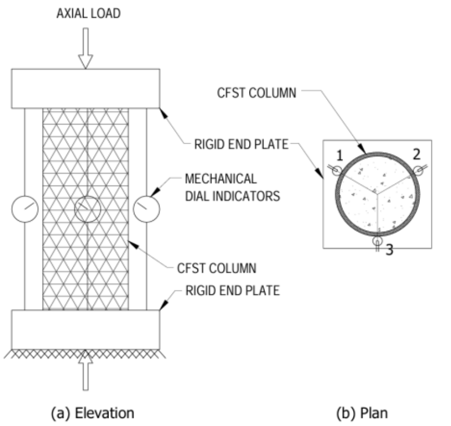

Fig. 5 Schematic instrumentation diagram

2.2 Results and discussions

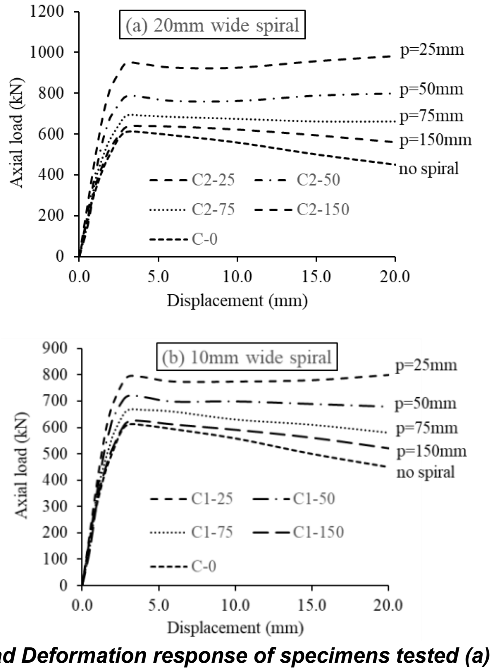

Fig. 6 Load Deformation response of specimens tested (a) 20mm wide spiral (b) 10mm wide spiral

The ultimate load was defined as the load corresponding to the first peak in the load–deformation curve. Throughout testing, the load–displacement response of each specimen was carefully recorded. The ultimate loads and the corresponding strength ratios defined as the ratio of the ultimate load of a specimen with spiral plate stiffeners to that of the control specimen (C–0) are summarized in Table 1.

The axial load–displacement curves of all nine specimens are presented in Fig. 6. Figure 6(a) shows the response of specimens reinforced with 20 mm wide spiral plates, while Fig. 6(b) presents the behavior of specimens incorporating 10 mm wide spiral plates. The detailed discussion that follows first focuses on the 20 mm wide spiral specimens. All columns exhibited an initially steep and nearly linear increase in load up to an axial shortening of approximately 3–4 mm. This response indicates that the initial elastic stiffness was primarily governed by the composite interaction between the steel tube and the concrete core. During this stage, the presence of spiral plate stiffeners had minimal influence on stiffness, as both materials behaved integrally prior to significant concrete dilation or yielding of the steel tube. Beyond the elastic stage, distinct differences in structural response became evident. The control specimen (C–0) reached an ultimate load of 611 kN at an axial shortening of approximately 3 mm. After reaching the peak load, a gradual reduction in capacity was observed, with the load decreasing to approximately 450 kN at 20 mm displacement. This post-peak softening behavior is typical of conventional CFST columns, where outward local buckling of the steel tube and progressive crushing of the concrete core dominate the failure mechanism. Specimen C2–150, incorporating a 20 mm wide spiral with a pitch of 150 mm, exhibited only marginal improvement. The ultimate load increased to approximately 640 kN, corresponding to a 5% enhancement relative to the control specimen. Although post-peak softening was still observed, the residual strength at 20 mm displacement improved to about 560 kN. This indicates that a widely spaced spiral provides limited confinement and is insufficient to effectively restrain local buckling at larger deformations. As the spiral pitch decreased, the effectiveness of confinement became increasingly pronounced. Specimen C2–75 achieved an ultimate load of 692 kN, representing a 13% increase compared to C–0. Its post-peak response exhibited a near-plateau behaviour rather than significant softening, suggesting that moderate spiral spacing provided partial confinement and delayed the onset of local buckling. A further reduction in pitch to 50 mm (Specimen C2–50) resulted in a clear transition toward strain-hardening behaviour. The ultimate load increased to 787 kN, corresponding to a 29% improvement over the control specimen. Unlike the previous specimens, C2–50 did not experience strength degradation after peak load. Instead, the load remained stable and increased slightly, reaching approximately 800 kN at 20 mm displacement. This stable response demonstrates that a 50 mm spiral pitch provides continuous and effective confinement, thereby maintaining strong composite action between the steel tube and the concrete core. The most significant enhancement was observed in specimen C2–25, incorporating a tightly spaced 20 mm wide spiral with a 25 mm pitch. This specimen reached an ultimate load of 948 kN, representing a 55% increase compared to C–0. Moreover, its post-peak behaviour remained highly stable, with the load remaining nearly constant—or slightly increasing—throughout the loading range, ultimately reaching approximately 982 kN at 20 mm displacement. The closely spaced spiral effectively restrained lateral expansion of the concrete, inducing a triaxial compressive stress state that significantly enhanced both strength and ductility. In addition, the spiral acted as a continuous internal stiffener, reducing the effective buckling length of the steel tube wall and preventing outward local buckling even at large deformations.

A similar trend was observed for specimens reinforced with 10 mm wide spiral plates, as shown in Fig. 6(b). In all cases, reducing the spiral pitch led to increased ultimate strength, improved post-peak stability, and enhanced confinement efficiency. However, for a given pitch, specimens with 20 mm wide spirals consistently exhibited higher strength and better load retention compared to those with 10 mm wide spirals, highlighting the significant influence of plate width on confinement effectiveness.

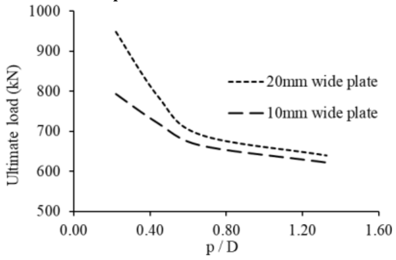

Fig. 7 Variation of ultimate axial load with the normalized spiral pitch

Figure 7 illustrates the variation of ultimate axial load with the normalized spiral pitch (p/D), where p is the spiral pitch and D is the outer diameter of the steel tube. Two curves are presented: one corresponding to specimens reinforced with 20 mm wide spiral plates and the other to specimens with 10 mm wide spiral plates. A clear decreasing trend in ultimate load is observed for both plate widths as p/D increases. For the 20 mm wide spiral plates, the highest ultimate load is achieved at the smallest normalized pitch (p/D ≈ 0.25), with a capacity of approximately 950kN. As p/D increases to about 1.3–1.4, the ultimate load decreases to nearly 640kN, representing a substantial reduction in strength. A similar trend is observed for the 10 mm wide spiral specimens, although the corresponding ultimate loads are consistently lower than those of the 20 mm specimens across all pitch values. The significant strength enhancement at small p/D values is attributed to the improved confinement of the concrete core and the effective restraint against outward local buckling of the steel tube provided by closely spaced spiral plates. A smaller pitch increases the number of confinement points along the column height, inducing a triaxial compressive stress state in the concrete core and enhancing composite interaction between the steel tube and concrete. In contrast, as the spiral pitch increases, the spacing between restraint points becomes larger, reducing confinement efficiency. Consequently, the structural response gradually approaches that of an unstiffened CFST column. From the overall trend of both curves, a threshold value of approximately p/D ≈ 0.5 can be identified. Below this value, the ultimate load increases sharply with decreasing pitch, indicating highly effective confinement. Beyond this limit, the rate of strength enhancement diminishes, and the benefit of further pitch reduction becomes less pronounced. Therefore, spiral pitches corresponding to p/D ≤ 0.5 are recommended to achieve substantial strength improvement in circular CFST columns.

The ductility of CFST columns was evaluated using the strain degradation rate, defined as the change in load relative to the corresponding change in axial strain. A lower or negative strain degradation rate indicates superior ductility and stable post-peak behaviour, whereas a higher positive value signifies rapid stiffness degradation and a more brittle response. The strain degradation rates presented in Table 1 indicate that the incorporation of internal plate spiral stiffeners improved the ductility of the CFST columns. The effect of spiral pitch was evident, with closer spiral spacing resulting in superior ductile behaviour. For the 10 × 2 mm plate series, the strain degradation rate increased from -2.7×10^{-6} for C1-150 to 0.1×10^{-6} for C1-25. A similar trend was observed for the 20 × 2 mm plate series, where the value increased from -2.1×10^{-6} for C2-150 to 0.8×10^{-6} for C2-25. The improved ductility is attributed to the enhanced confinement provided by the spiral plates, which delayed local buckling of the steel tube and promoted gradual stress redistribution within the composite section. Specimens with wider spiral plates (20 × 2 mm) generally exhibited better ductility than those with narrower plates (10 × 2 mm), indicating the beneficial effect of increased confinement.

The deformed shape of two test specimens is shown in Fig. 14. The control specimen (C–0) and specimens with larger spiral pitches exhibited pronounced outward local bulging of the steel tube. Deformation was concentrated between intermittent weld locations, indicating insufficient lateral restraint. The widely spaced spirals were unable to provide continuous confinement, allowing the steel tube to buckle outward and the concrete core to expand laterally, which reduced confinement effectiveness and led to post-peak strength degradation. As the spiral pitch decreased, the spacing between stiffener plates reduced, effectively limiting local buckling of the tube wall. For the tightest pitch (25mm), the spiral provided near-continuous internal support, resulting in minimal buckling amplitude and uniformly distributed deformation along the column height. The enhanced confinement maintained the integrity of the steel tube, delayed concrete crushing, and produced higher axial strength with stable post-peak behavior. Moreover, for a given pitch, specimens with 20 mm wide spiral plates consistently demonstrated superior confinement efficiency compared to 10 mm wide plates, highlighting the important role of plate width in improving composite action.

3. Finite Element Study

To complement the experimental investigation, a detailed finite element modeling (FEM) study was conducted using the commercial software ABAQUS. The numerical model was developed to simulate the axial behavior of circular concrete-filled steel tube (CFST) columns incorporating internal spiral plate stiffeners, with the primary objective of assessing their confinement effectiveness and composite interaction mechanisms. The finite element model was first calibrated against the experimental load–displacement responses to ensure accuracy and reliability. Key parameters, including material constitutive models, contact interactions, and boundary conditions, were adjusted to achieve close agreement with the test results. Once validated, an extensive parametric study was performed to evaluate the influence of spiral pitch, plate width, and material properties on the structural performance of stiffened CFST columns. The steel tube and spiral plates were modeled using appropriate nonlinear material properties to capture yielding and strain hardening behavior. For the concrete core, the Concrete Damaged Plasticity (CDP) model available in ABAQUS was adopted to represent the nonlinear compressive and tensile behavior of concrete, including stiffness degradation due to cracking and crushing. The key CDP parameters include the dilation angle (Ψ), the ratio of the initial equibiaxial compressive yield stress to the initial uniaxial compressive yield stress (f_{b0}/f_c'), and the parameter K_c, which defines the shape of the yield surface in the deviatoric plane. In the present study, (f_{b0}/f_c') was taken as 1.16, while a value of 0.66 was adopted for K_c , consistent with values widely used in previous studies. Within the CDP framework, the dilation angle (Ψ) is a critical parameter governing the volumetric expansion of concrete under compression. This parameter significantly influences the confinement interaction between the expanding concrete core and the surrounding steel tube. A higher dilation angle generally results in increased lateral pressure development and enhanced confinement effects. In the present study, the dilation angle was determined using the empirical relationship proposed by Alrebeh and Ekmekyapar (2019a), as given in Eq. (1).

$$\Psi = \begin{cases} 56.3(1-\xi_c) & \text{for } \xi_c \le 0.5 \\ 6.672 e^{\frac{7.4}{4.64+\xi_c}} & \text{for } \xi_c > 0.5 \end{cases} \tag{1}$$

ξ_c is the confinement index and is given by Eq (2).

$$\xi_c = \frac{A_s f_y}{A_c f_c'} \tag{2}$$

where A_s is the cross-sectional area of steel tube, A_c is the cross-sectional area of concrete core, f_y is the yield stress of steel tube and f_c' is the cylinder compressive strength of concrete. Compressive and tensile damage variables represent the progressive degradation of concrete stiffness due to crushing and cracking, respectively. The compressive damage parameter (d_c) and tensile damage parameter (d_t) were calculated based on the effective concept adopted in ABAQUS as given by Eq (3) and (4), respectively.

$$d_c = 1 - \sigma_c / \{E_0(\varepsilon_c - \varepsilon_c^{pl})\} \tag{3}$$

$$d_t = 1 - \sigma_t / \{E_0(\varepsilon_t - \varepsilon_t^{pl})\} \tag{4}$$

where σ_c and σ_t are the compressive and tensile stresses, respectively; E_0 is the initial elastic modulus of concrete; $\varepsilon_c$and ε_t are the total compressive and tensile strains; and ε_c^{pl} and ε_t^{pl} are the corresponding plastic strains. For the numerical simulation, elements with reduced integration points were used to accurately capture nonlinear material behavior. The steel tube, being thin-walled, was modeled using S4R elements, which are four-noded shell elements with reduced integration, applied specifically at nodal points to capture local buckling and bending effects efficiently. On the other hand, the concrete core was represented using C3D8R elements which are 8-noded linear brick elements with reduced integration points. The selection of element sizes is a critical aspect of the modeling process and was determined based on the desired output accuracy and the optimization of the analysis time. In this case, an element size within the range of 10mm to 15mm was chosen for all the specimens. Fig. 8 illustrates the geometric model of a typical column. Fig. 8(a) shows the shell and Fig. 8(b) indicates the concrete core.

The interaction between the steel tube and the concrete core was modeled using a surface-to-surface contact formulation, as it critically governs composite action and load transfer. A friction coefficient of 0.25 was assigned in the tangential direction, following Tao et al. (2016), while a hard contact condition was adopted in the normal direction to prevent interpenetration under compression and allow separation under tension. The intermittent welds between the spiral plates and the steel tube were simulated using tie constraints at the designated weld locations, ensuring full force transfer. The connection between the spiral plates and the concrete core was modeled using the embedded element technique in ABAQUS, enabling bonded interaction.

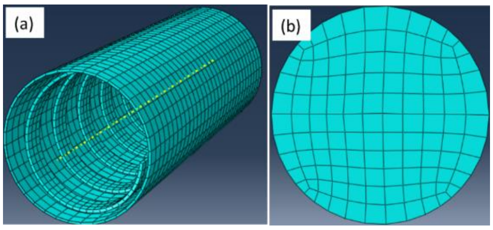

Fig. 8 Typical column model

3.1 Boundary Conditions

The boundary conditions were defined to realistically simulate the experimental setup. The top end of the specimen was modeled as free to move along the longitudinal (vertical) direction, while the bottom end was fixed to represent its support on the foundation. To achieve this, two translational degrees of freedom at the top and three translational degrees of freedom at the bottom were restrained, preventing any unintended lateral displacements. A multi-point constraint (MPC), available within ABAQUS, was employed to implement these boundary conditions effectively. This feature allows multiple nodes to be linked to a reference point, ensuring uniform displacement and accurate representation of real support behavior. The final configuration of the boundary conditions is illustrated in Fig. 9.

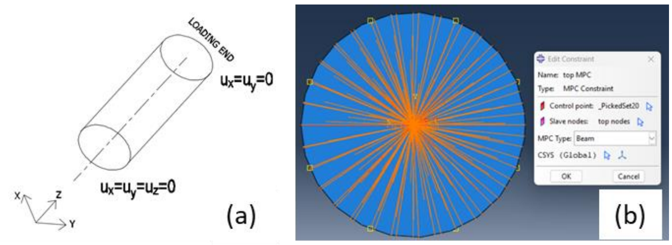

Fig. 9 Boundary conditions (a) Schematic view (b) MPC constraints

3.2 Material Modelling of Steel

In the numerical analysis, the Poisson's ratio of the steel tube was assumed to be 0.3, and the elastic modulus (E_s) was set at 200 GPa. The yield stress of both the steel tube and the spiral plate stiffeners was taken as given by the respective authors. To accurately model the nonlinear mechanical behaviour of the steel components, a stress–strain relationship proposed by Tao et al. (2013) was adopted. This constitutive model effectively represents the elastic, yielding, and strain-hardening stages of structural steel.

$$\sigma = \begin{cases} E_s & 0 \le \varepsilon \le \varepsilon_y \\ f_y & \varepsilon_y \le \varepsilon < \varepsilon_p \\ f_u - (f_u - f_y)\left(\varepsilon_u - \varepsilon / \varepsilon_u - \varepsilon_p\right)^p & \varepsilon_p \le \varepsilon < \varepsilon_u \\ f_u & \varepsilon \ge \varepsilon_u \end{cases} \quad (5)$$

Here f_y is the yield stress, ε_y is the yield strain, f_u is the ultimate stress, ε_u is the ultimate strain, ε_p is the strain at the start of strain hardening. The calculation of various terms is given below.

$$p = E_p\left(\frac{\varepsilon_u - \varepsilon_p}{f_u - f_y}\right) \quad (6)$$

$$E_p = 0.02E_s \quad (7)$$

$$\varepsilon_p = \begin{cases} 15\varepsilon_y & f_y \le 300MPa \\ \left(15 - 0.018(f_y - 300)\right)\varepsilon_y & 300MPa < f_y \le 800MPa \end{cases} \quad (8)$$

$$\varepsilon_u = \begin{cases} 100\varepsilon_y & f_y \le 300MPa \\ \left(100 - 0.15(f_y - 300)\right)\varepsilon_y & 300MPa < f_y \le 800MPa \end{cases} \quad (9)$$

A typical plot of the stress strain model is shown in Fig. 10a.

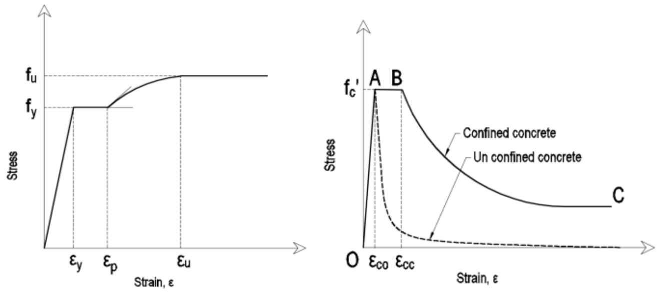

Fig. 10 Stress strain model of (a) steel material (b) confined concrete material

3.3 Material Modelling of Concrete

In the material modelling process, nonlinear stress–strain data for confined concrete is incorporated, following the recommendations of Tao et al. (2013). The adopted stress–strain relationship is illustrated in Fig. 10b. For the purpose of comparison, a standard stress–strain curve for unconfined concrete is also presented in the same diagram. This comparison highlights the enhanced strength and ductility provided by the confinement effect in CFST columns.

The initial portion OA is taken exactly same as that of unconfined concrete and is described as,

$$\frac{\sigma}{f_c'} = \frac{A.X + B.X^2}{1 + (A-2)X + (B+1)X^2} \quad for\ 0 < \varepsilon < \varepsilon_{c0} \quad (10)$$

Where σ is the stress in concrete corresponding to a strain ε. f_c' is the compressive cylinder strength of concrete. $X = \frac{\varepsilon}{\varepsilon_{c0}}$, $A = \frac{E_c \varepsilon_{c0}}{f_c'}$, $B = \frac{(A-1)^2}{0.55} - 1$. Here ε_{c0} is the strain corresponding to point A of the graph and is expressed in terms of cylinder strength by De Nicolo *et al.* (1994),

$$\varepsilon_{c0} = 0.00076 + \sqrt{(0.626f_c' - 4.33)x10^{-7}} \quad (11)$$

E_c is the modulus of elasticity of concrete and is taken as $E_c = 4700\sqrt{f_c'}$

The strain at point B, ε_{cc} is given by Samani and Attard (2012),

$$\frac{\varepsilon_{cc}}{\varepsilon_{c0}} = e^k \quad (12)$$

$$\text{where } k = (2.9224 - 0.00367f_c')\left(\frac{f_B}{f_c'}\right)^{0.3124 + 0.002f_c'} \quad (13)$$

Here f_B is the confining stress

$$f_B = \frac{(1 + 0.027f_y)e^{-0.02\frac{D}{t}}}{1 + 1.6e^{-10}(f_c')^{4.8}} \text{ for circular sections} \quad (14)$$

The portion BC of the curve is adopted as proposed by Binici (2005) which is given below,

$$\sigma = f_{res} + (f_c' - f_{res})exp\left[-\left(\frac{\varepsilon - \varepsilon_{cc}}{\alpha}\right)^\beta\right] \text{ for } \varepsilon \ge \varepsilon_{cc} \quad (15)$$

where f_{res} is the residual stress in concrete.

$$f_{res} = \begin{cases} 0.7\left(1 - e^{-1.38\xi_c}\right)f_c' \le 0.25f_c' & \text{for circular sections} \\ 0.1f_c' & \text{for square sections} \end{cases} \quad (16)$$

$$\alpha = \begin{cases} 0.04 - \frac{0.036}{1 + e^{6.08\xi_c - 3.49}} & \text{for circular sections} \\ 0.005 + 0.0075\xi_c & \text{for square sections} \end{cases} \quad (17)$$

Value of β is taken as 1.2 for circular sections.

3.4 Validation of the FE Model

The finite element (FE) model was validated using both the experimental results from the present study and additional data reported by other researchers, as summarized in Table 2. The comparison focused on two key aspects (1) Load–deformation response, as shown in Fig. 11, and (2) Ultimate axial load, as presented in Table 2. The results indicate a strong agreement between the FE simulations and experimental data, demonstrating that the developed numerical model accurately captures the structural behavior of CFST columns with internal spiral stiffeners.

Table 2. Comparison of Ultimate load

Author	Specimen ID	Ultimate load (kN)		Variation
		Experiment (N_{ue})	Prediction using FE (N_{uFE})	$\frac{N_{ue} - N_{uFE}}{N_{ue}} x100$
Present study	C1-25	794	745	6%
	C1-50	721	705	2%
	C1-75	666	695	-4%
	C1-150	623	658	-6%
	C2-25	948	902	5%
	C2-50	787	777	1%
	C2-75	692	710	-3%
	C2-150	640	668	-4%
Alrebeh & Ekmekyapar (2019b)	C-IS-8-7	1400	1277	+9%
	C-IS-8-5	1294	1255	+3%
	C-IS-8-3	1098	1048	+5%
Arokiaprakash & Senthil (2023)	CPC-S-25t	550	582	-6%

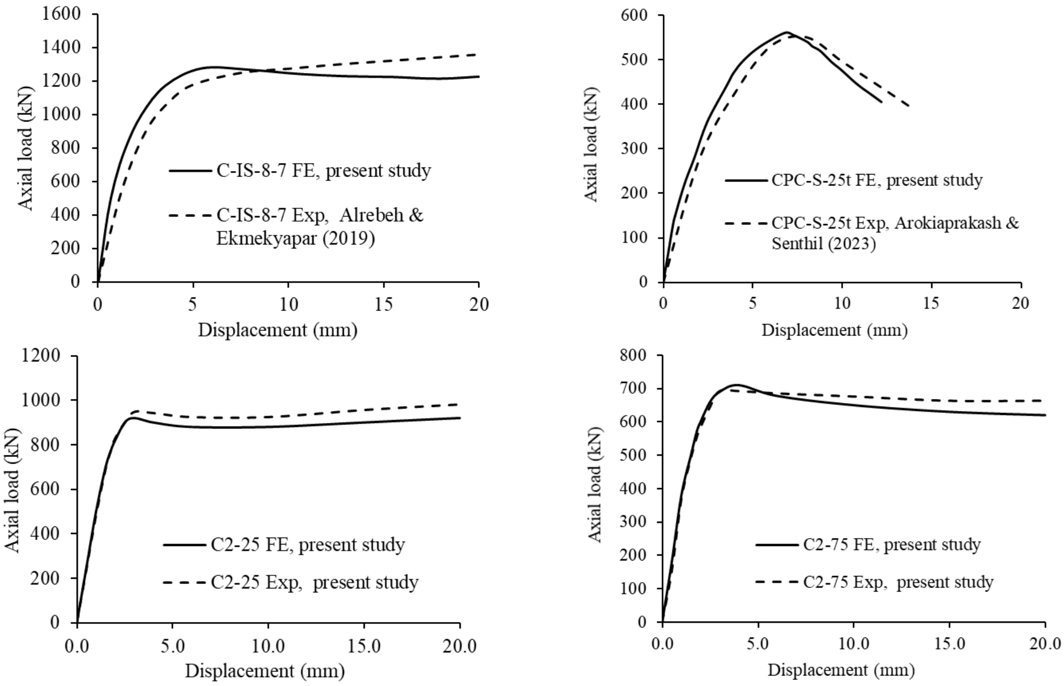

Fig. 11 Load-deformation comparison of finite element values with experimental values

4. Parametric Study

A comprehensive investigation was carried out to understand the behavior of confined CFST columns by considering multiple influencing parameters. The variables examined in this study are detailed in Table 3 and include tube diameter, tube thickness, spiral pitch, spiral plate size, weld spacing, and concrete grade. The yield stresses of the steel tube and the spiral plate stiffeners were taken as 290 MPa and 260 MPa, respectively. A total of 22 specimens were analyzed through finite element (FE) simulations, as summarized in Table 4, covering all the aforementioned variables. Among these, specimens C1 to C15 represent CFST columns with internal spiral plate stiffeners, while specimens C16 to C22 serve as control columns without stiffeners.

Table 3. Variables considered in the analysis

Parameter	Variables
Tube diameter, D	100mm, 150mm, 200mm,
Tube thickness, t	1mm, 2mm, 3mm
Pitch of spiral, p	25mm, 50mm, 75mm, 100mm
Size of spiral plate, b_s	20x2, 30x2, 40x2mm
Weld spacing, s_w	30, 45, 90, 180 degrees
Grade of concrete, f_c	20, 40, 60 MPa

Table 4. Details of analysis specimens

Sl No	Specimen ID	Tube outer Dia, mm	Tube thickness, mm	Concrete strength, MPa	Weld spacing, degree	Spiral width, mm	Spiral thickness, mm	Pitch, mm	No of turns	Ultimate load, N_{FE}, kN
1	C1	100	2	40	45	30	2	50	6	697
2	C2	150	2	40	45	30	2	50	6	1367
3	C3	200	2	40	45	30	2	50	6	2248
4	C4	150	1	40	45	30	2	50	6	1149
5	C5	150	3	40	45	30	2	50	6	1734
6	C6	150	2	20	45	30	2	50	6	851
7	C7	150	2	60	45	30	2	50	6	1665
8	C8	150	2	40	30	30	2	50	6	1373
9	C9	150	2	40	90	30	2	50	6	1344
10	C10	150	2	40	180	30	2	50	6	1215
11	C11	150	2	40	45	20	2	50	6	1231
12	C12	150	2	40	45	40	2	50	6	1399
13	C13	150	2	40	45	30	2	25	12	1767
14	C14	150	2	40	45	30	2	75	4	1241
15	C15	150	2	40	45	30	2	100	3	1200
16	C16	100	2	40	45	-	-	-	-	575
17	C17	150	2	40	45	-	-	-	-	1148
18	C18	200	2	40	45	-	-	-	-	1848
19	C19	150	2	20	45	-	-	-	-	784
20	C20	150	2	60	45	-	-	-	-	1548
21	C21	150	1	40	45	-	-	-	-	994
22	C22	150	3	40	45	-	-	-	-	1555

4.1 Load Deformation response

The load–deformation responses of the CFST specimens under different parameter variations are shown in Fig. 12. All specimens exhibit a similar initial linear elastic behaviour, indicating effective composite action between the steel tube and the concrete core at early stages of loading. The ultimate load is generally reached at an axial strain of approximately 0.5%, after which the behaviour varies significantly depending on the parameter being considered. Specimens with effective confinement mechanisms show stable post-peak behaviour or strain hardening, whereas those with insufficient confinement exhibit softening and a rapid reduction in axial load capacity.

Effect of Tube Diameter: Fig. 12(a) illustrates the influence of tube diameter. Increasing the diameter results in a significant enhancement of ultimate load and residual strength. Specimen C3, with the largest diameter, exhibits superior performance compared to C1 and C2. A larger diameter increases the concrete core area, thereby improving the axial load-carrying capacity. Moreover, for a fixed spiral pitch, a larger diameter effectively reduces the normalized pitch ratio p/D, leading to improved confinement.

Effect of Tube Thickness: The effect of tube thickness is presented in Fig. 12(b). Specimen C5, with the thickest tube, shows the highest ultimate load and demonstrates a stable plateau with slight strain hardening after the peak. Thinner tubes, such as in specimen C4, exhibit more pronounced post-peak softening. Increased wall thickness enhances hoop stiffness and delays local buckling, allowing the steel tube to maintain effective confinement over a larger deformation range. Thicker tubes also contribute greater axial load resistance due to higher steel yield capacity, promoting ductile rather than brittle failure.

Effect of Concrete Strength: The influence of concrete grade is depicted in Fig. 12(c). Higher-strength concrete, as in specimen C7, results in a higher ultimate load compared to lower-strength concrete (C6). The baseline specimen C2 lies between the two. Although higher-strength concrete tends to be more brittle, the presence of adequate confinement provided by the spiral plates and steel tube ensures ductile behaviour, preventing sudden crushing of the core. These results confirm that higher-strength concrete can be effectively utilized in CFST columns, provided sufficient confinement is ensured.

Effect of Weld Spacing: Fig. 12(d) shows the effect of weld spacing, which determines the degree of interaction between the spiral plates and the steel tube. Specimens with closer weld spacing, such as C8, exhibit higher ultimate loads and more stable post-peak behaviour, whereas specimen C10, with widely spaced welds, shows premature softening and a significant loss of load-carrying capacity. Closer weld spacing enhances shear transfer between the spiral plates and the tube, allowing the spirals to act as continuous restraints. Conversely, larger weld gaps result in unsupported regions, where local bulging can occur, reducing the effectiveness of confinement.

Effect of Spiral Plate Width: The effect of spiral plate width is shown in Fig. 12(e). Increasing the plate width from 20mm to 40mm results in a substantial improvement in both peak strength and post-peak performance. Wider plates provide greater contact area between the spiral and the concrete, improving bond strength and shear transfer. They also increase the bending stiffness of the spiral, making it more effective at restraining the steel tube. This leads to enhanced triaxial confinement of the concrete core and delayed local buckling of the tube. A strength increase of approximately 22% is observed when the plate width is expanded to 40 mm.

Effect of Spiral Pitch: The most significant influence is observed in Fig. 12(f), which examines the effect of spiral pitch. Specimen C13, with the smallest pitch (25 mm), achieves the highest ultimate load and demonstrates excellent post-peak behaviour, characterized by a stable plateau and strain hardening. In contrast, specimens with larger pitches, such as C14 (75 mm) and C15 (100 mm), show reduced ultimate loads and more pronounced softening. Reducing the pitch increases the number of restraint points along the column length, providing near-continuous confinement of the concrete. A normalized pitch ratio $\boldsymbol{p/D}$≤0.5 is identified as a practical design threshold to achieve effective confinement and superior axial load performance.

Comparisons across all parameters indicate that spiral pitch is the most influential factor governing the axial performance of CFST columns with spiral plate stiffeners. Wider spiral plates and reduced weld spacing further improve confinement and post-peak behaviour. While higher-strength concrete increases peak capacity, it must be complemented by adequate confinement to prevent brittle failure. Optimizing geometric parameters such as pitch, plate width, and weld spacing is critical for maximizing the effectiveness of confinement and ensuring stable, ductile behaviour under axial compression.

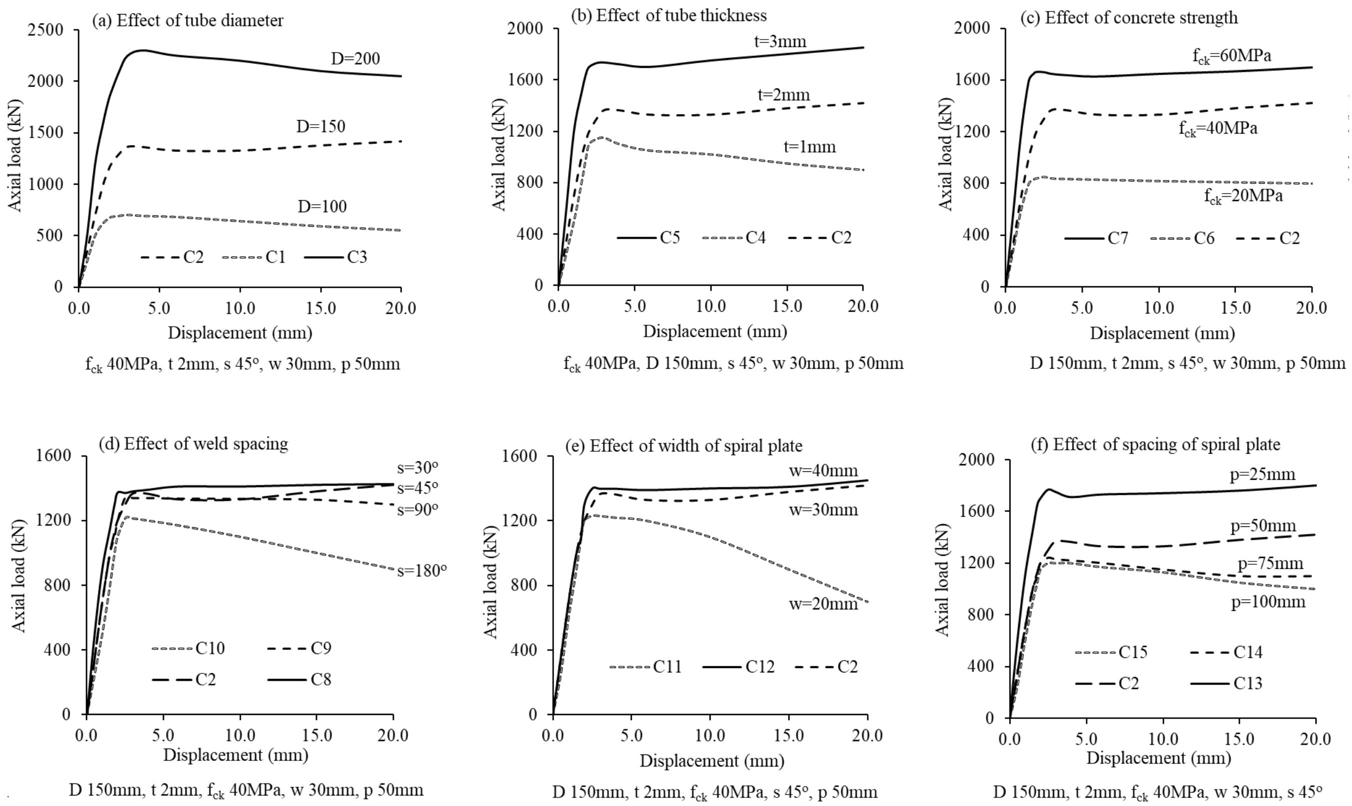

Fig. 12 Load deformation response of confined CFST columns having different (a) Tube diameter (b) Tube thickness (c) Concrete strength (d) Weld spacing (e) Width of spiral plate (f) Spacing of spiral plate.

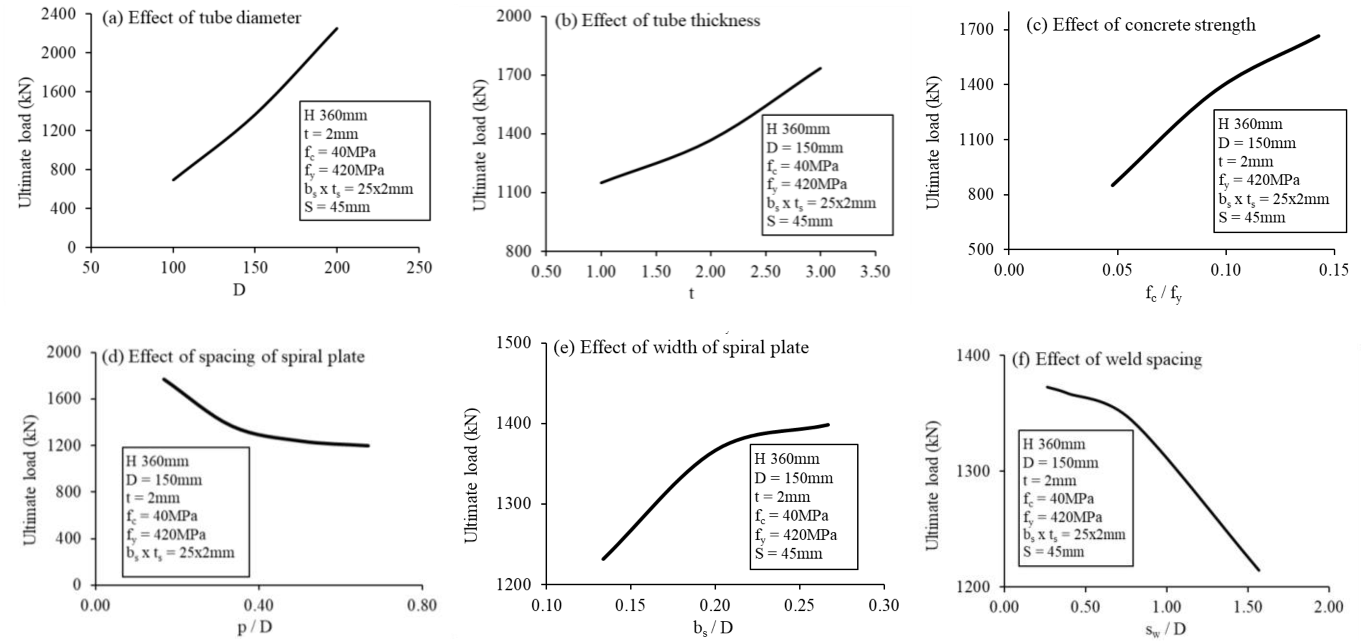

Fig. 13 Effect of various parameters on ultimate strength of column (a) Effect of tube diameter (b) Effect of tube thickness (c) Effect of concrete strength (d) Effect of spacing of spiral plate (e) Effect of width of spiral plate (f) Effect of weld spacing

4.2 Ultimate load

Table 5. The ultimate load and Strength ratio of columns

Sl No	Specimen ID	Ultimate load, N_{FE}, kN	Control specimen ID	Strength ratio
1	C1	697	C16	1.21
2	C2	1367	C17	1.19
3	C3	2248	C18	1.22
4	C4	1149	C21	1.16
5	C5	1734	C22	1.12
6	C6	851	C19	1.09
7	C7	1665	C20	1.08
8	C8	1373	C17	1.20
9	C9	1344	C17	1.17
10	C10	1215	C17	1.06
11	C11	1231	C17	1.07
12	C12	1399	C17	1.22
13	C13	1767	C17	1.54
14	C14	1241	C17	1.08
15	C15	1200	C17	1.05
16	C16	575	-	-
17	C17	1148	-	-
18	C18	1848	-	-
19	C19	784	-	-
20	C20	1548	-	-
21	C21	994	-	-
22	C22	1555	-	-
			Mean	1.16

The influence of various parameters on the ultimate load of column is studied and presented in graphical form in Fig. 13.

The finite element results clearly demonstrate the beneficial effect of internal spiral stiffening on the ultimate load of CFST columns. The strength ratio was calculated as the ratio of the ultimate load of a stiffened column to the ultimate load of its corresponding control specimen. The ultimate loads, associated control specimen IDs, and strength ratios are summarized in Table 5. Columns reinforced with spiral plates exhibited higher ultimate strengths compared to the corresponding control specimens. An average strength ratio of 1.16 was obtained, indicating that internal spiral stiffening provides a significant improvement in axial load capacity. A maximum increase in ultimate load of 54% is observed for the column C17. A comparison of specimens with different diameters (C1–C3 against C16–C18) indicated that the load-carrying capacity increases proportionally with tube diameter. However, the strength ratios remained nearly constant (1.19–1.22), suggesting that spiral stiffeners are equally effective across a wide range of diameters. Variations in tube thickness, as examined in C4 and C5, revealed that thinner tubes derived greater benefit from stiffeners (ratio 1.16 for 1 mm thickness vs. 1.12 for 3 mm thickness). This highlights that spiral stiffeners are particularly advantageous in thinner tubes, where the risk of local buckling is more critical. The effect of concrete strength was studied through specimens C6 and C7. Although a higher concrete grade (60 MPa) resulted in higher ultimate loads, the relative benefit of stiffening was less pronounced compared to lower grade concrete (20 MPa). This trend suggests that spiral stiffeners contribute more significantly when the confinement demand is higher, as in lower strength concrete. Spiral angle played a decisive role in the performance of stiffened specimens. At moderate angles (30–45°), the specimens exhibited the highest strength ratios (1.20–1.22). Increasing the spiral inclination to 90° and 180° reduced the confinement effect, leading to lower efficiency (1.17 and 1.06, respectively). Width of spiral plate also influenced the column ultimate load. While specimen C11 with smaller width (20 mm) achieved only marginal improvement (1.07), specimen C12 with wider plate (40 mm) achieved a considerably higher ratio (1.22). The most remarkable improvement was observed in specimen C13, where a pitch of 25 mm and 12 turns produced a strength ratio of 1.54, significantly higher than all other cases. This indicates that an optimum pitch exists, which maximizes confinement and efficiently redistributes stress. Beyond this point, as observed in specimens C14 and C15, the benefits diminished considerably.

4.3 Deformed shape of specimens

The deformed shapes of selected CFST column specimens with varying spiral plate pitches are presented in Fig. 14. Specimen C17, which does not contain spiral plate stiffeners, exhibited continuous outward buckling of the steel tube along its entire height. This global outward bulging occurred because there was no internal restraint to limit the lateral expansion of the concrete core or the steel tube wall. As a result, the column failed prematurely due to severe local buckling and loss of confinement. For specimens fitted with spiral plate stiffeners (C15, C14, C2, and C13), the deformation pattern changed significantly. The spiral plates, which were intermittently fillet-welded to the inner surface of the steel tube, acted as internal restraints, reducing excessive outward bulging. For the specimen C15 (Pitch = 100 mm) the outward bulging was primarily concentrated between the widely spaced spiral rings, creating distinct localized buckling zones. The restraint provided was minimal, and the deformation pattern remained similar to C17, although slightly less severe. In specimen C14 (Pitch = 75 mm) the bulging became less pronounced and more evenly distributed along the height of the column. The closer spiral spacing offered improved confinement, delaying the onset of local buckling and providing moderate control over lateral expansion.

Whereas for specimen C2 (Pitch = 50 mm) the deformation was further reduced, with outward bulging being significantly restrained. The spiral provided near-continuous confinement, ensuring that the steel tube deformation remained stable and more uniform. In case of specimen C13 (Pitch = 25 mm) the column displayed minimal and uniform deformation, with almost no distinct outward bulging. The very tight spiral spacing created continuous confinement, preventing the steel tube from buckling locally and maintaining the integrity of the composite section even under high axial loads. In general, as the spiral pitch decreases, the confinement provided by the spiral plates increases, leading to a more uniform distribution of deformations and a substantial reduction in local bulging. This effect is amplified by the intermittent weld spacing, which matches the spiral pitch and directly influences the transfer of forces between the steel tube, spiral plates, and concrete core.

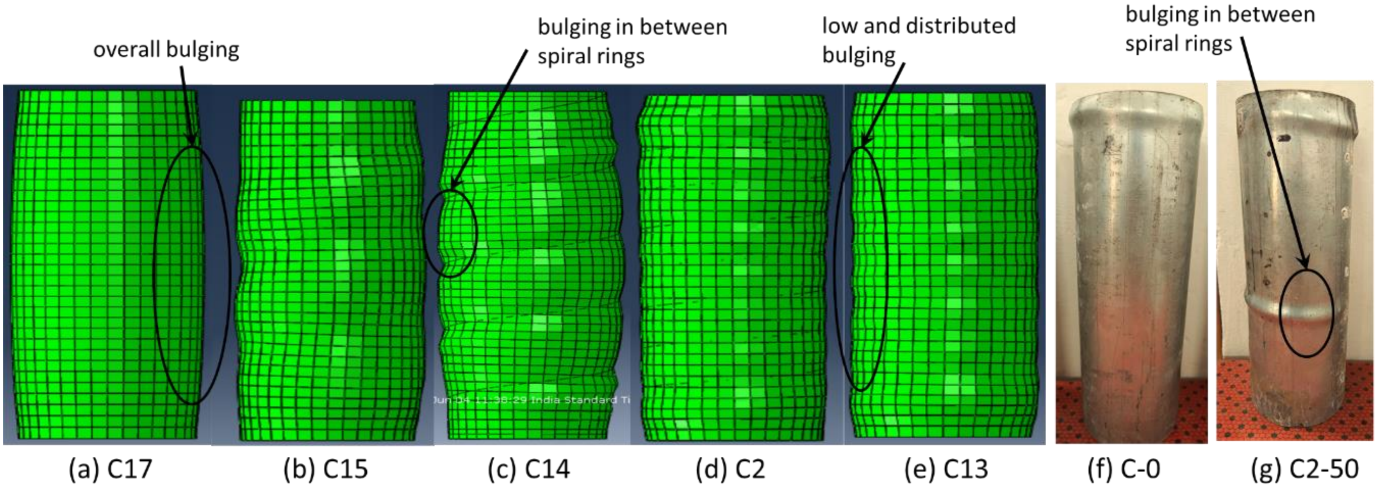

Fig. 14 Deformed shape of specimens with different spacing of plate spirals (a) without spiral-FE (b) 100mm spacing-FE (c) 75mm spacing-FE (d) 50mm spacing-FE (e) 25mm spacing-FE (f) without spiral – experimental (g) 50mm spacing - experimental

5. Ultimate Load Prediction Models

Table 6. Comparison of FE results with prediction models

Sl No	Specimen ID	N_{FE} (kN)	$N_{alrebeh}$ (kN)	$N_{FE}/N_{alrebeh}$	N_{zhou} (kN)	N_{FE}/N_{zhou}	N_{ACI} (kN)	N_{FE}/N_{ACI}	N_{EC4} (kN)	N_{FE}/N_{EC4}
1	C1	697	778	0.90	919	0.76	441	1.58	546	1.28
2	C2	1367	1309	1.04	1621	0.84	899	1.52	1095	1.25
3	C3	2248	2008	1.12	2478	0.91	1514	1.48	1805	1.24
4	C4	1149	1102	1.04	1359	0.85	804	1.43	902	1.27
5	C5	1734	1531	1.13	1838	0.94	993	1.75	1284	1.35
6	C6	851	1018	0.84	1286	0.66	564	1.51	775	1.10
7	C7	1665	1627	1.02	1958	0.85	1234	1.35	1419	1.17
8	C8	1373	1309	1.05	1621	0.85	899	1.53	1095	1.25
9	C9	1344	1309	1.03	1621	0.83	899	1.50	1095	1.23
10	C10	1215	1309	0.93	1621	0.75	899	1.35	1095	1.11
11	C11	1231	1237	1.00	1469	0.84	899	1.37	1095	1.12
12	C12	1399	1382	1.01	1775	0.79	899	1.56	1095	1.28
13	C13	1767	1310	1.35	2094	0.84	899	1.97	1095	1.61
14	C14	1241	1308	0.95	1469	0.84	899	1.38	1095	1.13
15	C15	1200	1308	0.92	1395	0.86	899	1.33	1095	1.10
16	C16	575	708	0.81	695	0.83	441	1.30	546	1.05
17	C17	1148	1264	0.91	1247	0.92	899	1.28	1095	1.05
18	C18	1848	1977	0.94	1981	0.93	1514	1.22	1805	1.02
19	C19	784	1059	0.74	989	0.79	564	1.39	775	1.01
20	C20	1548	1486	1.04	1464	1.06	1234	1.25	1419	1.09
21	C21	994	972	1.02	890	1.12	804	1.24	902	1.10
22	C22	1555	1584	0.98	1596	0.97	993	1.57	1284	1.21
Mean				1.02		0.83		1.45		1.18

Two existing models, namely the Alrebeh 2019 model (Alrebeh and Ekmekyapar, 2019b) and the Zhou 2023 model (Lin and Zhou, 2023), are used to predict the ultimate load of spirally confined CFST columns. Both models were originally developed for circular spiral cross-sections. However, no prediction models currently exist in the literature for spiral plate stiffeners. In the present study, these two models are modified to account for CFST columns stiffened with spiral plates. In the modification, the cross-sectional area of the circular spiral rod is replaced with the product $\boldsymbol{b_s t_s}$ (where $\boldsymbol{b_s}$ is the plate width and $\boldsymbol{t_s}$ is the plate thickness).

5.1 Prediction by Alrebeh 2019 model

The free body diagram of the confined column is shown in Fig. 15a

Confinement index is,

$$\xi = A_{st}\sigma_{sy}/A_c f_c' \tag{18}$$

Where,

$$A_{st} = A_s + \frac{b_s t_s}{H}\left(2\pi\left(D - \frac{b_s}{2}\right) + n\sqrt{S^2 + \left(\pi^2\left(D - \frac{b_s}{2}\right)\right)}\right)\frac{\sigma_{spy}}{\sigma_{sy}} \tag{19}$$

Hoop stress is to be calculated using,

$$\frac{\sigma_{s\theta}}{\sigma_{sy}} = \begin{Bmatrix} 0 & 0 \le \xi < 0.03 \\ -0.003\xi^2 + 0.175\xi - 0.006 & 0.03 \le \xi < 2.5 \\ 0.244 & \xi \ge 2.5 \end{Bmatrix} \tag{20}$$

As per Von-Mises failure criterion,

$$\sigma_{s\theta}^2 + \sigma_{s\theta} + \sigma_{sz}^2 = \sigma_{sy}^2 \tag{21}$$

The confining pressure is calculated by,

$$f_r = \sigma_{s\theta}\frac{2t}{D-2t} + \sigma_{spy}\frac{4b_s t_s}{H(D-2t)} + \sigma_{spy} cos\left[arc\ tan\left(\frac{S}{\pi\left(D-\frac{b_s}{2}\right)}\right)\right]\frac{2b_s t_s}{S(D-2t)} \tag{22}$$

Find the confined compressive stress of concrete,

$$f_{cc} = f'_c + Kf_r = f'_c + 3.16f_r \tag{23}$$

Hence the ultimate compressive strength of confined CFST column can be calculated by,

$$N_{alrebeh} = f_{cc}A_c + \sigma_{sz}A_s + 2n\sigma_{spy}b_s t_s sin\left[arctan\left(\frac{S}{\pi\left(D-\frac{b_s}{2}\right)}\right)\right] \tag{24}$$

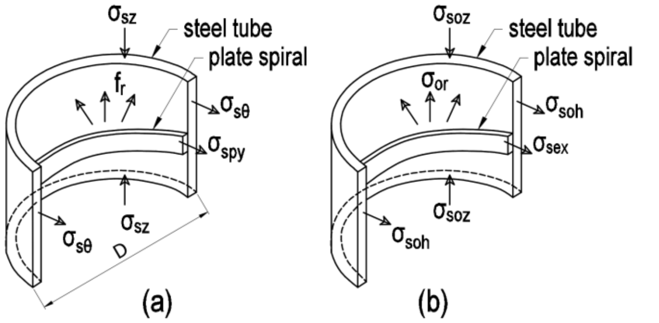

Fig. 15 Free body diagram of CFST column confined by plate spiral (a) Alrebeh 2019 model, (b) Zhou 2023 model

5.2 Prediction by Zhou 2023 model

The free body diagram of the confined column is shown in Fig. 15b . The external confining pressure provided by steel spirals can be calculated by

$$\sigma_{sexr} = \sigma_{sex}.\cos[arctan(S/(\pi(D_o - b_s/2)))]2b_s t_s/(S(D_o - 2t_o)) \quad (25)$$

The axial compressive component contribution of spiral plates is calculated by

$$N_{uex} = \sigma_{sex}.\sin[arctan(S/(\pi(D_o - b_s)/2))]\, b_s t_s \quad (26)$$

Hoop stress in the steel tube is

$$\sigma_{soh} = \beta f_{yo} \quad (27)$$

Where,

$$\beta = -0.2(D_o/t_o)^{0.35}(f_c/f_{yo})^{0.45} \quad (28)$$

The external pressure confining from the steel tube is written as

$$\sigma_{sor} = -2t_o./(Do - 2t_o)\,.\,\sigma_{soh} \quad (29)$$

Summation of all the external confining pressures acting on the outer surface of core concrete is obtained as

$$\sigma_{or} = \sigma_{sor} + \sigma_{sexr} \quad (30)$$

The longitudinal compressive stress in the steel tube σ_{soz}can be obtained from Von Mises yield criterion

$$\sigma_{soz}{}^2 - \sigma_{soz}.\sigma_{soh} + \sigma_{soh}{}^2 = f_{yo}{}^2 \quad (31)$$

The value of σ_{soz} shall not be less than elastic local buckling stress σ_{sob} of a steel tube having concrete infill. Lai *et al*. (2017) and (2020) suggested the value of σ_{sob} as,

$$\sigma_{sob} = 90\sqrt{3}\frac{235}{D_o/t_o} \quad (32)$$

The triaxial compressive strength of infilled concrete is

$$f_{cpa} = f_c(1 + 4.138(\sigma_{or}/f_c)^{1.101}) \quad (33)$$

Ultimate uniaxial compressive strength of column is

$$N_{zhou} = f_{cpa}A_c + \sigma_{soz}A_{so} + N_{uex} \quad (34)$$

The ultimate loads calculated using the ACI 318 provisions, Eurocode 4 (EC4) provisions, Alrebeh (2019) model and Zhou (2023) model were compared with the FE analysis results and are presented in Table 6. The ultimate strengths predicted by the models are graphically compared with the FE results in Fig. 16. The mean strength ratios obtained were N_{FE}/N_{ACI} = 1.45, N_{FE}/N_{EC4} = 1.18, $N_{FE}/N_{alrebeh}$ = 1.02, and N_{FE}/N_{zhou} = 0.83, with corresponding standard deviations of 0.18, 0.14, 0.12, and 0.07, respectively. The ACI model exhibited the largest deviation from the FE results, overestimating the axial strength by approximately 45%. This can be attributed to the fact that the ACI provisions do not explicitly account for the confinement mechanism in CFST columns and are therefore unable to accurately represent the interaction between the steel tube, concrete core, and internal plate spiral. The EC4 model provided improved predictions, with an average underestimation of approximately 18%, as it incorporates the confinement effect of conventional circular CFST columns. However, the additional confinement generated by the internal plate spiral stiffener is not explicitly considered in the EC4 formulation. Among the models considered, the Alrebeh (2019) model provided the closest agreement with the FE results, with a mean strength ratio of 1.02 and a relatively low standard deviation of 0.12. The improved accuracy of this model may be attributed to its confinement formulation, which better represents the contribution of spiral confinement to the composite action of the CFST column. Although the Zhou (2023) model exhibited the lowest standard deviation (0.07), it consistently overestimated the axial strength, resulting in a mean strength ratio of 0.83. The comparison indicates that analytical models that explicitly incorporate the confinement effect of internal spiral stiffeners provide more accurate predictions of the axial strength of CFST columns than conventional design code provisions.

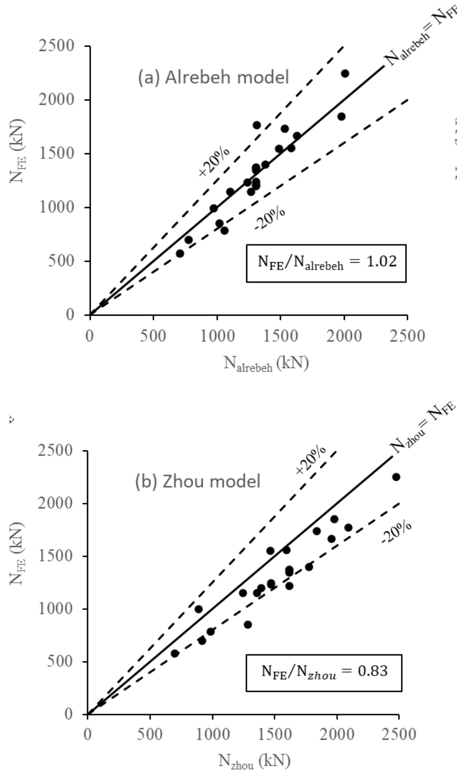

Fig. 16 Comparison of FE strength with predicted strength

6. Conclusions

This study proposed a new confinement technique for circular concrete-filled steel tube (CFST) columns using internal rectangular spiral plate stiffeners attached to the inner surface of the steel tube through intermittent external plug welding. The structural behavior was investigated experimentally under axial compression and validated through detailed finite element modeling. Existing strength prediction models were further modified to account for the contribution of spiral plate stiffeners. Based on the experimental and numerical investigations, the following conclusions can be drawn:

a. The incorporation of internal spiral plate stiffeners resulted in an average ultimate strength enhancement of approximately 16% compared to conventional CFST columns without stiffeners.
b. The ultimate strength increased by 5% to 55% as the spiral pitch decreased from 150 mm to 25 mm. Similarly, reducing weld spacing from 180° to 30° improved strength by 6% to 20%. A normalized spiral pitch (p/D) ≤ 0.5 was found to provide effective and continuous confinement, significantly enhancing axial load capacity, delaying local buckling, and ensuring stable post-peak behaviour. Increasing the spiral plate width up to 40 mm led to a strength enhancement of approximately 22%.
c. Spiral plate stiffeners effectively delayed outward local bulging of the steel tube. As the spiral pitch decreased, deformation became more uniformly distributed along the column height, resulting in improved structural stability.
d. The modified axial strength prediction models showed good agreement with finite element results, indicating their suitability for practical design applications of circular CFST columns incorporating spiral plate stiffeners.

References

Abbas, N. J., & Ali, A. A. (2021). Prediction of axial capacity of octagonal concrete-filled steel tube columns considering confinement effect. Int. J. Struct. Eng., 12(2), 170-188. https://doi.org/10.1504/IJSTRUCTE.2022.121891

Alrebeh, S. K., Ahmed, A. D., Al-Asad, A. K., & Ekmekyapar, T. (2023). Experimental performance evaluation of concrete-filled steel tube columns confined by high-strength steel bolts. Int. J. Steel Struct., 23(4), 1135-1147. https://doi.org/10.1007/s13296-023-00755-x

Alrebeh, S. K., & Ekmekyapar, T. (2019b). Structural performance of short concrete-filled steel tube columns with external and internal stiffening under axial compression. Structures, 20, 702-716. https://doi.org/10.1016/j.istruc.2019.06.015

Alrebeh, S. K., & Ekmekyapar, T. (2019a). Structural behavior of concrete-filled steel tube short columns stiffened by external and internal continuous spirals. Structures, 22, 98-108. https://doi.org/10.1016/j.istruc.2019.07.001

Arokiaprakash, A., & Selvan, S. (2022). An experimental behavior of the bond-slip performance of hybrid fiber concrete-filled steel tube columns with shear studs. Asian Journal of Civil Engineering, 24, 1-13. https://doi.org/10.1007/s42107-022-00510-3

Arokiaprakash, A., & Senthil, S. S. (2023). Comprehensive study of compressive behavior of CFST columns with confinements and stiffeners. J. Constr. Steel Res., 211, 108127. https://doi.org/10.1016/j.jcsr.2023.108127

Binici, B. (2005). An analytical model for stress-strain behavior of confined concrete. Eng. Struct., 27(7), 1040-1051. https://doi.org/10.1016/j.engstruct.2005.03.002

Chen, J., Yang, Z. M., Hu, L., & Wang, J. (2023). Behavior of CFRP confined circular CFST columns reinforced with internal latticed steel angles under seismic loading. J. Constr. Steel Res., 208, 108033. https://doi.org/10.1016/j.jcsr.2023.108033

Dabaon, M., El-Khoriby, S., El-Boghdadi, M., & Hassanein, M. F. (2009). Confinement effect of stiffened and unstiffened concrete-filled stainless-steel tubular stub columns. J. Constr. Steel Res., 65(8-9), 1846-1854. https://doi.org/10.1016/j.jcsr.2009.04.012

de Oliveira, W. L. A., De Nardin, S., De Cresce, E. L. H., & El Debs, M. K. (2010). Evaluation of passive confinement in CFT columns. J. Constr. Steel Res., 66(4), 487-495. https://doi.org/10.1016/j.jcsr.2009.11.004

Giakoumelis, G., & Lam, D. (2004). Axial capacity of circular concrete-filled tube columns. J. Constr. Steel Res., 60, 1049-1068. https://doi.org/10.1016/j.jcsr.2003.10.001

Gupta, A., Mohan, R., Bisht, H., & Sharma, A. (2022). Experimental testing and numerical modelling of CFST columns under axial compressive load. Asian Journal of Civil Engineering, 23(3), 415-424. https://doi.org/10.1007/s42107-022-00432-0

Guptha, P. K., Khaudhair, Z. A., & Ahuja, A. K. (2014). Computational study on performance of circular concrete-filled steel tubular columns. Int. J. Struct. Eng., 5(1), 76-91. https://doi.org/10.1504/IJSTRUCTE.2014.058685

Guptha, P. K., Verma, V. K., Khaudhair, Z., & Singh, H. (2015). Effect of tube area on the behavior of concrete-filled tubular columns. Compt. Concrete, 15(2), 141-166. https://doi.org/10.12989/cac.2015.15.2.141

Hamed, E., Younas, S., Li, D., & Uy, B. (2021). Behaviour of high strength concrete-filled short steel tubes under sustained loading. Steel Compos. Struct., 39(2), 159-170. https://doi.org/10.12989/scs.2021.39.2.159

Hoang, A. L., & Fehling, E. (2017). Numerical analysis of circular steel tube confined UHPC stub columns. Compt. Concrete, 19(3), 263-273. https://doi.org/10.12989/cac.2017.19.3.263

Hu, C., Wang, Y., Cheng, R., Luo, J., & Gong, M. (2024). Confinement effect and stress-strain model for concrete of multi-cell CFST column under axial compression. J. Constr. Steel Res., 221, 108865. https://doi.org/10.1016/j.jcsr.2024.108865

Hu, Y. M., Yu, T., & Teng, J. G. (2011). FRP-confined circular concrete-filled thin steel tubes under axial compression. J. Compos. Constr., 15(5), 850-860. https://doi.org/10.1061/(ASCE)CC.1943-5614.0000217

Huang, C. S., Yeh, Y. K., Liu, G. Y., Hu, H. T., Tsai, K. C., Weng, Y. T., Wang, S. H., & Wu, M. H. (2002). Axial load behavior of stiffened concrete-filled steel columns. J. Struct. Eng., 128(9), 1222-1230. https://doi.org/10.1061/(ASCE)0733-9445(2002)128:9(1222)

Lai, M. H., & Ho, J. C. M. (2014). Behaviour of uni-axially loaded concrete-filled-steel-tube columns confined by external rings. Struct. Design Tall Spec. Build., 23(6), 403-426. https://doi.org/10.1002/tal.1051

Lai, M. H., & Ho, J. C. M. (2014). Confinement effect of ring-confined concrete-filled-steel-tube columns under uni-axial load. Eng. Struct., 67, 123-141. https://doi.org/10.1016/j.engstruct.2014.02.013

Lai, M. H., & Ho, J. C. M. (2015). Axial strengthening of thin-walled concrete-filled-steel-tube columns by circular steel jackets. Thin-Walled Struct., 97, 11-21. https://doi.org/10.1016/j.tws.2015.09.002

Lai, M. H., & Ho, J. C. M. (2015). Effect of continuous spirals on uni-axial strength and ductility of CFST columns. J. Constr. Steel Res., 104, 235-249. https://doi.org/10.1016/j.jcsr.2014.10.007

Li, S., Liu, F., Chan, T.-M., Yang, H., & Young, B. (2025). Novel concrete-filled steel square tubular columns stiffened with semi-circles: Concept and behaviour. Thin-Walled Structures, 212, 113188. https://doi.org/10.1016/j.tws.2025.113188

Lin, C., & Zhou, J. (2023). Axial compressive behaviour of circular composite columns with external confinement. J. of Build. Eng., 77, 107516. https://doi.org/10.1016/j.jobe.2023.107516

Lyu, F., Ding, F., Xu, Q., & Sun, H. (2024). Refined finite element modelling of circular CFST bridge piers subjected to the seismic load. Compt. Concrete, 33(6), 643-658. https://doi.org/10.12989/cac.2024.33.6.643

Midhin, A. K., Nabilah, A. B., Nazir, N. A. M., & Safiee, N. A. (2020). Bond behaviour in rubberised concrete-filled circular steel tubes. Int. J. Struct. Eng., 10(4), 293-306. https://doi.org/10.1504/IJSTRUCTE.2020.109850

Naghipour, M., Khalili, A., Hasani, S. M. R., & Nematzadeh, M. (2022). Experimental investigation of natural bond behavior in circular CFTs. Steel Compos. Struct., 42(2), 191-207. https://doi.org/10.12989/scs.2022.42.2.191

Nematzadeh, M., & Fazli, S. (2020). Effect of axial loading conditions and confinement type on concrete-steel composite behavior. Compt. Concrete, 25(2), 95-109. https://doi.org/10.12989/cac.2020.25.2.095

Petrus, C., Hamid, H. A., Ibrahim, A., & Parke, G. (2010). Experimental behaviour of concrete-filled thin-walled steel tubes with tab stiffeners. J. Constr. Steel Res., 66(7), 915-922. https://doi.org/10.1016/j.jcsr.2010.02.006

Prabhu, G. G., & Sundarraja, M. C. (2013). Behaviour of concrete-filled steel tubular (CFST) short columns externally reinforced using CFRP strips composite. Constr. Build. Mater., 47, 1362-1371. https://doi.org/10.1016/j.conbuildmat.2013.06.038

Samani, A. K., & Attard, M. M. (2012). A stress-strain model for uniaxial and confined concrete under compression. Eng. Struct., 41, 335-349. https://doi.org/10.1016/j.engstruct.2012.03.027

Schneider, S. P. (1998). Axially loaded concrete-filled steel tubes. J. Struct. Eng., 124(10), 1125-1138. https://doi.org/10.1061/(ASCE)0733-9445(1998)124:10(1125)

Tao, Z., Han, L. H., & Wang, D. Y. (2007). Experimental behaviour of concrete-filled stiffened thin-walled steel tubular columns. Thin-Walled Struct., 45(5), 517-527. https://doi.org/10.1016/j.tws.2007.04.003

Tao, Z., Han, L. H., & Wang, D. Y. (2008). Strength and ductility of stiffened thin-walled hollow steel structural stub columns filled with concrete. Thin-Walled Struct., 46(10), 1113-1128. https://doi.org/10.1016/j.tws.2008.01.007

Tao, Z., Han, L. H., & Wang, Z. B. (2005). Experimental behaviour of stiffened concrete-filled thin-walled hollow steel structural (HSS) stub columns. J. Constr. Steel Res., 61(7), 962-983. https://doi.org/10.1016/j.jcsr.2004.12.003

Tao, Z., Song, T. Y., Uy, B., & Han, L. H. (2016). Bond behavior in concrete-filled steel tubes. J. Constr. Steel Res., 120, 81-93. https://doi.org/10.1016/j.jcsr.2015.12.030

Tao, Z., Uy, B., Han, L. H., & Wang, Z. B. (2009). Analysis and design of concrete-filled stiffened thin-walled steel tubular columns under axial compression. Thin-Walled Struct., 47(12), 1544-1556. https://doi.org/10.1016/j.tws.2009.04.010

Tao, Z., Wang, Z.-B., & Yu, Q. (2013). Finite element modelling of concrete-filled steel stub columns under axial compression. J. of Constr. Steel Res., 89, 121-131. https://doi.org/10.1016/j.jcsr.2013.07.001

Thomas, J., & Sandeep, T. N. (2018) Experimental study on circular CFST short columns with intermittently welded stiffeners. Steel Compos. Struct., 29 (5), 659-667. https://doi.org/10.12989/scs.2018.29.5.659

Thomas, J., & Sandeep, T. N. (2020) Capacity of short circular CFST columns with inner vertical plates welded intermittently. J. Constr. Steel Res., 165, 105840. https://doi.org/10.1016/j.jcsr.2019.105840

Winti, A. C., Abdullah, A. A., Abdul Karim, A. R., Kueh, A. B. H., & Bronny, B. G. (2026). Axial compressive behavior of square CFST short columns with steel plate reinforcement. Asian Journal of Civil Engineering, 27, 3099-3122. https://doi.org/10.1007/s42107-026-01658-y

Zhu, B., Li, X., & Yang, D. (2026). Axial compression behaviour of square concrete-filled steel tube columns with stiffeners and multi-spiral stirrups. Structures, 85, 111198. https://doi.org/10.1016/j.istruc.2026.111198

Disclaimer